Exp Astron (2012) 33:237–269
DOI 10.1007/s10686-011-9260-3

ORIGINAL ARTICLE

Solar Particle Acceleration Radiation and Kinetics (SPARK)

A mission to understand the nature of particle acceleration

Sarah A. Matthews · David R. Williams · Karl-Ludwig Klein · Eduard P. Kontar · David M. Smith · Andreas Lagg · Sam Krucker · Gordon J. Hurford · Nicole Vilmer · Alexander L. MacKinnon · Valentina V. Zharkova · Lyndsay Fletcher · Iain G. Hannah · Philippa K. Browning · Davina E. Innes · Gerard Trottet · Clare Foullon · Valery M. Nakariakov · Lucie M. Green · Herve Lamoureux · Colin Forsyth · David M. Walton · Mihalis Mathioudakis · Achim Gandorfer · Valentin Martinez-Pillet · Olivier Limousin · Erwin Verwichte · Silvia Dalla · Gottfried Mann · Henri Aurass · Thomas Neukirch

Received: 31 March 2011 / Accepted: 14 September 2011 / Published online: 18 October 2011

S. A. Matthews (✉) · D. R. Williams · L. M. Green ·
H. Lamoureux · C. Forsyth · D. M. Walton
UCL Mullard Space Science Laboratory, Holmbury St. Mary, Dorking RH5 6NT, UK
e-mail: sam@mssl.ucl.ac.uk

K.-L. Klein · N. Vilmer · G. Trottet
LESIA, Observatoire de Paris-Meudon, Paris, France

E. P. Kontar · A. L. MacKinnon · L. Fletcher · I. G. Hannah
SUPA, School of Physics & Astronomy,
University of Glasgow, Glasgow, UK

D. M. Smith
UC Santa Cruz, Santa Cruz, CA, USA

A. Lagg · D. E. Innes · A. Gandorfer
MPS, Lindau, Germany

S. Krucker
UC Berkeley, Berkeley, CA, USA

S. Krucker
University of Applied Sciences, North Western Switzerland (FHNW), Windisch, Switzerland

G. J. Hurford
Space Sciences Lab. UC Berkeley, Berkeley, CA, USA

V. V. Zharkova
University of Bradford, Bradford, UK

Abstract Energetic particles are critical components of plasma populations found throughout the universe. In many cases particles are accelerated to relativistic energies and represent a substantial fraction of the total energy of the system, thus requiring extremely efficient acceleration processes. The production of accelerated particles also appears coupled to magnetic field evolution in astrophysical plasmas through the turbulent magnetic fields produced by diffusive shock acceleration. Particle acceleration is thus a key component in helping to understand the origin and evolution of magnetic structures in, e.g. galaxies. The proximity of the Sun and the range of high-resolution diagnostics available within the solar atmosphere offers unique opportunities to study the processes involved in particle acceleration through the use of a combination of remote sensing observations of the radiative signatures of accelerated particles, and of their plasma and magnetic environment. The SPARK concept targets the broad range of energy, spatial and temporal scales over which particle acceleration occurs in the solar atmosphere, in order to determine how and where energetic particles are accelerated. SPARK combines highly complementary imaging and spectroscopic observations of radiation from energetic electrons, protons and ions set in their plasma and magnetic context. The payload comprises focusing-optics X-ray imaging covering the range from 1 to 60 keV; indirect HXR imaging and spectroscopy from 5 to 200 keV, γ-ray spectroscopic imaging with high-resolution $LaBr_3$ scintillators, and photometry and source localisation at far-infrared wavelengths. The plasma environment of the regions of acceleration and interaction will be probed using soft X-ray imaging of the corona and vector magnetography of the photosphere and chromosphere. SPARK is designed for solar research. However,

P. K. Browning
University of Manchester, Manchester, UK

C. Foullon · V. M. Nakariakov · E. Verwichte
University of Warwick, Conventry, UK

M. Mathioudakis
Queen's University Belfast, Belfast, UK

V. Martinez-Pillet
Instituto de Astrofisica de Canarias, La Laguna, Tenerife, Spain

O. Limousin
CEA Saclay, Gif-sur-Yvette, France

S. Dalla
UCLan, Preston, UK

G. Mann · H. Aurass
AIP, Potsdam, Germany

T. Neukirch
University of St. Andrews, St. Andrews, UK

in addition it will be able to provide exciting new insights into the origin of particle acceleration in other regimes, including terrestrial gamma-ray flashes (TGF), the origin of γ-ray bursts, and the possible existence of axions.

Keywords Sun: atmosphere · Particle acceleration · Space missions: instruments · ESA Cosmic vision

1 Introduction

Particle acceleration occurs in many and diverse sites throughout the universe e.g., stellar coronae, active galactic nuclei, the coronae of accretion disks around black holes, the magnetospheres of neutron stars, and planetary atmospheres interacting with the wind of their star, including the Earth's. The processes involved are highly efficient: in transient energy release the accelerated particle energy represents a large fraction of the total energy released. Magnetic field evolution and particle acceleration are closely coupled, through the conversion of free magnetic energy to particle energy and the interaction of plasma flow and energetic particles, which can lead to magnetic field amplification. For example, Bamert et al. [2] has found direct evidence for the self-generation of magnetohydrodynamic (MHD) turbulence in heliospheric shocks, and recent observations of supernova remnants (SNRs) provide strong support for magnetic field amplification in the shock waves associated with cosmic ray acceleration (e.g. Vink et al. [59] and references therein). Thus, not only do the pervasive energetic particles impact, e.g., planetary environments, the processes involved also play a key role in shaping magnetic structure throughout the universe. Particle acceleration is a key scientific issue in answering questions related to how our own and other solar systems work; what the conditions for planet formation and the emergence of life are, and what the universe is made of.

The Sun is the most efficient particle accelerator in the solar system, capable of accelerating ions to energies from a few MeV to tens of GeV, and electrons from tens of keV to tens of MeV, on timescales of 100–1,000 s. The accelerated electron component of solar flares contains up to 50% of the total energy released, while solar energetic particle (SEP) events contain ∼10% of the total energy of the associated coronal mass ejection (CME), for those events accompanied by a CME. How and where these particles are accelerated and the details of the processes producing such a wide range of energies remains to be fully understood. Our ability to probe many layers of the solar atmosphere simultaneously with high spatial, spectral and temporal resolution offers unique opportunities to study the relationship between fundamental physical processes such as magnetic reconnection, wave generation and particle acceleration. These are the same processes also operating in other astrophysical environments. It is the proximity of the Sun that provides us with the broad range of high-resolution radiative signatures of energetic particles that are available in the solar atmosphere. Only here can we observe their

time evolution, and map the evolving magnetic field configuration where the acceleration takes place.

The most direct radiative signatures of energetic particles are γ-rays—produced by nuclear reactions of ions and by electron bremsstrahlung; bremsstrahlung hard X-rays, and a broad range of radio emissions probably reaching into the so far unobserved far-infrared range. Other ranges of the electromagnetic spectrum also carry signatures of energetic particles, but these are less direct. Solar physics has exploited diagnostics over a broad band of wavelengths, starting with radio waves in the 1940s. Hard X-ray spectroscopy of solar flares started in the late 1950s from balloons [44], the first gamma-ray spectroscopic observations were made in 1980 [8]. Since the late 1970s a fleet of spacecraft has developed our observational knowledge of hard X-ray and γ-ray emissions, including the solar-dedicated ISEE3, *Solar Maximum Mission* (SMM), *Hinotori*, *Yohkoh* and CORONAS spacecraft, and the general astrophysics missions *Compton Gamma-Ray Observatory*, *GAMMA*, *GRANAT*, *INTEGRAL* and *FERMI*. The *Ramaty High Energy Solar Spectroscopic Imager* (RHESSI) has been operating since 2002, making the first images of solar flares in a nuclear γ-ray line.

Through decades of investigations our picture of the role of energetic particles in the solar atmosphere has evolved from the idea that particle acceleration is an exceptionally energetic phenomenon in some flares to the insight that energetic particles are seen in nearly every manifestation of magnetic energy conversion, from large flares down to minor explosive events in active regions and sometimes even the quiescent solar atmosphere. The evaluation of the energy budget of flares suggests that non-thermal electrons, and probably also protons, carry a significant fraction of the energy released, and that the flare is a fundamentally non-thermal process. Electromagnetic radiation is produced during flares by electrons and ions accelerated to largely suprathermal, occasionally relativistic energies in a time of the order of seconds or less. This occurs where the magnetic field changes topology, releasing stored energy. The SPARK concept targets the entire range of the solar particle acceleration, from suprathermal electrons to relativistic ions. The payload includes a photospheric and chromospheric imaging vector magnetograph to provide inputs for extrapolations that will help determine the magnetic field in the corona in which the particles are accelerated, as well as details of the impact sites and field evolution in the lower atmosphere during the precipitation of the accelerated particles; soft X-ray imaging of hot thermal plasma ($>10^6$ K) that will allow us to better constrain the relationship between thermal and non-thermal emission; direct HXR imaging with high dynamic range that will allow us to image e.g. loop-top and footpoint HXR sources within the same field-of-view, as well as HXR emission from non-flaring active regions; complementary high resolution, time resolved HXR and γ- ray imaging spectroscopy that will provide details of the energy spectra of the accelerated electrons and ions and their evolution; and the first measurements from space of the far infrared (FIR) component of solar flares which will allow us to probe the highest energy

particles accelerated in the solar atmosphere. In particular, SPARK is designed to answer the following over-arching questions:

- What is the role of the magnetic field in determining the onset and evolution of particle acceleration?
- How and where are energetic particles accelerated on the Sun?

Flares are of course not the only means by which the Sun accelerates particles. The shocks associated with CMEs are also highly efficient accelerators and these particles escape into the interplanetary medium to form SEP events. Of those accelerated by flares a significant fraction will remained trapped producing γ-ray emission observed in the solar atmosphere; but some will also escape. While the largest SEP events are perceived to arise through CME-related shock acceleration, there are large SEP events unaccompanied by CMEs and fast and wide CMEs with no associated SEP event. Thus there are major unanswered question in the study of SEPs, including the role of flare-accelerated particles in these events, and the details of the shock acceleration process in CMEs. Solar Orbiter and Solar Probe are specifically targeted at these questions and so we do not address them in detail here, but we emphasize that SPARK will have the capability to make significant contributions to this area by providing quantitative information about the energy and spectra of electrons during eruptive events, including shock-accelerated electrons in the low corona; quantifying the energy and spectra of trapped ions, and identifying the onset of eruptions and related shocks in the low corona.

The questions above are addressed in more detail in Section 2, and are complemented by a brief outline of science questions in other regimes, including terrestrial gamma-ray flashes, the origin of γ-ray bursts, and the possible existence of axions. The SPARK measurement strategy will be addressed in Section 3. The design of the individual instruments is described in Section 4. Section 5 outlines the spacecraft concept.

2 Scientific objectives

In the following sub-sections we expand some of the more detailed questions related to the over-arching science goals briefly listed above, emphasizing how SPARK can address these problems.

2.1 What is the role of the magnetic field in determining the onset and evolution of particle acceleration?

The magnetic field stores the energy and defines the environment in which it is released explosively in solar flares. A major component of the stored magnetic energy is converted into the kinetic energy of the accelerated particles. The initiation and evolution of the magnetic instability, the topology and the

subsequent evolution of the field, affect, and may dominate, the acceleration and transport of non-thermal particles.

The evolution of the HXR spectrum and the source positions show a clear link between the energization of electrons and the changing topology of the field. For example, anti-correlation between magnetic flux transfer rate and minimum overall spectral index [37], leads to harder spectra at the outer edges of (the rarely observed) HXR ribbons (e.g. [38, 40]). However, in practice, while some features of the HXRs are well described by current models, the picture overall is unclear. HXRs, like impulsive optical emission are restricted to compact footpoints, not ribbons as in Hα and (E)UV. Even taking into account the restricted dynamic range of current HXR imaging techniques this means that there are highly localised, preferential sites within the overall magnetic field structure where electron acceleration takes place, and which map onto these very compact footpoints.

To fully probe how reconnection in different magnetic environments affects the spatial, temporal and spectral properties of non-thermal particles requires a combination of high dynamic range, direct HXR imaging and HXR spectroscopy, complemented by optical and SXR imaging to confirm the location of energetic particle precipitation and validate the magnetic field extrapolation. This extrapolation must be carried out under realistic boundary conditions, which can only be provided by vector magnetic field measurements in both the photosphere and the chromosphere. The SPARK instruments have been chosen to provide coverage over a wide range of particle energies from electrons below 10 keV to ions above 1 GeV.

2.2 How and where are energetic particles accelerated on the Sun?

Particle acceleration processes in the solar atmosphere produce large numbers of energetic particles ranging from supra-thermal to relativistic energies. The solar atmosphere thus presents an excellent opportunity to understand how particles are accelerated on a myriad of scales—energetic, spatial and temporal. The SPARK instrumentation package has been chosen to provide almost complete coverage of the whole range of energies, and will target the areas outlined below:

2.2.1 Lower-energy extremes

Non-thermal electron signatures are not only found in conspicuous flares. Hard X-ray emission of very small flares [15, 34], the millimetre wave [32] and metre wave emission [3, 22, 47] associated with non-flaring active regions, and even radio emission from the quiet chromosphere [30] carry signatures of non-thermal electrons. Observations with increasing sensitivity to non-thermal electrons have shown increasing evidence that particle acceleration is intrinsic to the solar atmosphere, on many scales. Figure 1a illustrates this point using recent observations. It shows that despite contemporary observations being able to capture flares over six orders of X-ray magnitude, the smallest active

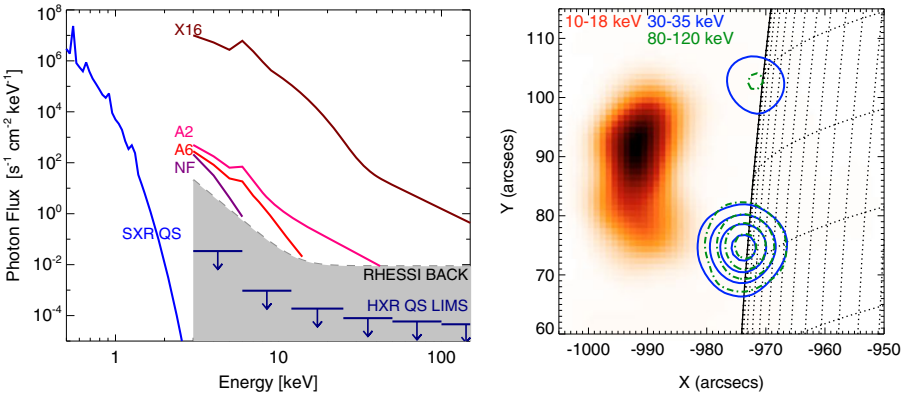

Fig. 1 **a** Model thermal and non-thermal spectra based on RHESSI observations of a large flare (X4.8) [18], microflares (A2, A6) [15] and non-flaring active regions (NF) [41]. For the quiet Sun a model thermal spectrum and RHESSI upper limits are included [16]. The *shaded region* indicates the emission beyond current observable limits. **b** RHESSI X-ray images of the January 6, 2004 limb flare [29]. The *contours* show hard X-ray emission integrated for the impulsive phase of the flare. Note that there is no hard X-ray emission from the flaring loop

region flares (A-Class) are badly affected by instrumental background, in all but exceptional cases (i.e. A2 event in Fig. 1a, [15]). The result is that the determination of the energetics in these small events is dominated by uncertainties. Observations beyond these instrumental limits would greatly improve the understanding of particle acceleration in the small events and possibly extend it to the even smaller active region flares recently observed in SXR. It would also allow us to quantify particle acceleration outside of the active regions in the quiet Sun, for which at the moment only long time averaged upper limits exist [16].

Understanding the physical processes in smaller events will also give crucial information on how widespread and important for the energetics of the solar atmosphere particle acceleration actually is. This is a basic question for the understanding of the solar atmosphere, where particle acceleration also operates in apparently quiescent environments. Studying acceleration of particles in smaller events will be key to assessing the nature of the energy conversion processes under different physical conditions.

One of the probes for the character of electron acceleration is the HXR time evolution. Flare-related HXR emission has a characteristic timing, including sub-second variations, and a characteristic spectral evolution, which most often consists of a hardening until the peak of the burst, followed by a softening. In order to pinpoint the similarities and differences of particle acceleration in phenomena ranging from large flares to nanoflares, one has to characterise spectral evolution and acceleration time scales, using spectrographic imaging across as extended a range of event sizes as possible. Although γ-ray observations will likely not pertain to low-energy events, the investigation of how far into the low-energy range the observed correlation between γ-ray and

HXR fluences extends will be an important element in the assessment of size-dependent similarities and differences of particle acceleration events.

Electrons at energies below 10–20 keV may contain the bulk of the total electron energy released during a flare, although this emission is dominated by the thermal emission from the heated corona, making the total electron energy difficult to determine. However, this low energy part of the electron spectrum is the one most affected by transport effects, such as wave-particle interactions and return currents. The electron acceleration rate above 20 keV is around 10^{37} s^{-1} in a large flare, which poses severe difficulties for understanding the electrodynamics of the beams. An understanding of how deka-keV electrons evolve is crucial to uncover the dominant processes for electron transport in solar flares, including the expected return current interactions, and hence provide the observations for new models beyond those relying on collisional transport.

While the energy spectrum of energetic electrons is relatively well known (with the exception of the low energy cut-off), our knowledge of the angular distribution of energetic electrons is very limited. In the standard flare scenario the accelerated electrons are beamed downwards. Since relativistic electrons emit in the direction of their propagation, this should be reflected in strong directivity and noticeable polarization of the emitted HXR (e.g. [33, 61]). HXR photons emitted downwards are also effectively scattered by the electrons in the photosphere (both free and bound) and hence a substantial fraction of HXRs will be back-scattered into the observer's direction. RHESSI observations have demonstrated that this Compton backscattering (X-ray albedo) can be detected in a spatially integrated spectrum via a broad bump in the range between 20 and 50 keV [28]. However, the observations are inconsistent with strong downward beaming of electrons [23, 27]. This dilemma questions the standard flare model, and can only be addressed with new albedo, directivity and X-ray polarization measurements. SPARK has the potential to provide the first images of the albedo component. These observations are crucial to constrain new physical modelling of the main processes leading to the formation of the observed angular distribution.

Why SPARK? The development of focusing optics at hard X-ray wavelengths now makes it possible to address weak signatures of non-thermal electrons. The SPARK concept includes HXR spectrographic imaging with increased sensitivity and dynamic range to identify non-thermal electron populations under various circumstances, including flares, active regions, and the apparently quiet solar atmosphere. In combination with SXR imaging, SPARK will provide new constraints on the transition between thermal and non-thermal plasma. SPARK will also be able to extend γ-ray observations to smaller events than before. Small and possibly simple events may present an ideal opportunity to study particle acceleration in simple magnetic configurations. The plasma of the chromosphere during a flare is heated by the energy transported from the primary energy release site in the corona. Thermal far-infrared (FIR) radiation from the heated chromosphere is a free-free contin-

uum that is easier to interpret than line emissions, enabling measurements of the energy deposited in deep atmospheric layers. Comparison of the HXR and γ-ray emission from non-thermal particles with the thermal FIR at sub-second resolution will allow us to distinguish between energy transport by conduction fronts and energetic particles. SPARK will make the first measurements from space in this wavelength regime.

2.2.2 High-energy extremes

The most direct quantitative diagnostics of energetic particles interacting at the Sun are provided by HXR/γ-ray observations. They give information on electron and ion energy spectra, numbers and energy contents (see Fig. 2). While bremsstrahlung X-ray continuum emission gives us information about energetic electrons, γ-ray lines from 0.4–8 MeV tell us about ions above a few MeV in energy and the continuum above 100 MeV yields information on ions >0.2 GeV/nuc (e.g. [48, 58]). Intriguingly, in a few large flares the energy content of ions above a few MeV is comparable to the energy of the electrons >20 keV as determined from the X-ray continuum (e.g. [42, 45, 46]). Because of the relatively low flux in the γ-ray range, our present knowledge of the acceleration histories of different particles during flares is extremely poor. SPARK offers enhanced sensitivity in this range and the opportunity to understand in detail the partitioning of energy between the various species in the flaring plasma.

Imaging of nuclear line emission at 2.23 MeV has been achieved by RHESSI for five events [58]. Statistically significant displacements between HXR and

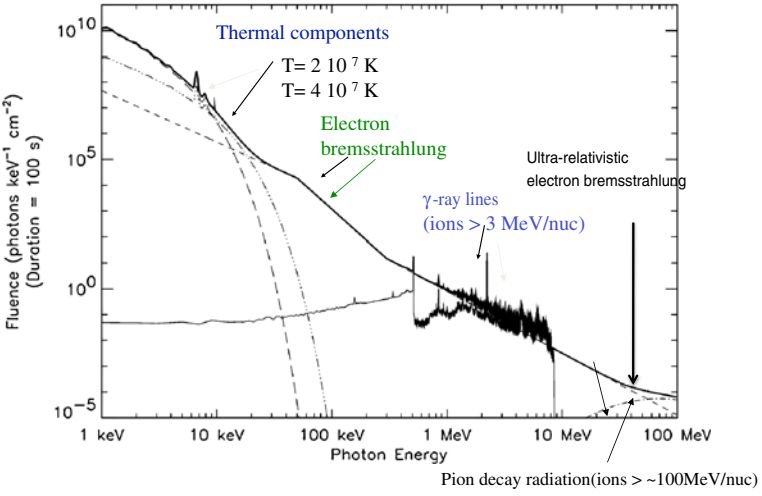

Fig. 2 The γ-ray spectrum from a solar flare, indicating the different emission components (adapted from the RHESSI web-site)

GRL sources were observed in three of these events. In four of the five events where nuclear line emission was imaged by RHESSI, a single unresolved source was observed in the GRL domain. Given the 36 arcsecond angular resolution of the imaging technique, this is not evidence that the inherent GRL line sources are predominantly single sources, a result that would be in stark contrast to typical hard X-ray double sources. Clearly though, our understanding of the displacement between the γ-ray and HXR source locations revealed by RHESSI is limited by the dynamic range and sensitivity of the imaging techniques. We have learned that species-dependent differences are intrinsic to the acceleration or transport of the particles, or both. Their understanding is a key element of particle acceleration, but we have so far only a glimpse at it.

γ-ray lines are not detected in all flares, even those where bremsstrahlung is observed above 10 MeV. While this does not exclude the production of energetic ions in these events [52, 56], it is important to understand whether the absence of a detection is the result of e.g. the hardness of the electron continuum above 300 keV, poor spectral resolution, or both. Ions below a few MeV/nuc are those whose energetics we need to compare with the thermal plasma and the accelerated electrons. A sensitive, low-background spectrometer such as that on-board SPARK can refine current estimates of fluence and line shapes for the already well-observed lines. In addition, MacKinnon [39] pointed out the possible diagnostic role of radiative capture lines, which are weak but sensitive to ions in the 0.1–1 MeV range. These diagnostics will be accessible with SPARK.

GeV protons have been shown for several decades to be present in large solar eruptive events by ground-based neutron monitors. The γ-ray emission from similarly high-energy protons and neutrons above 100 MeV was first detected aboard SMM/GRS [7, 58]. The existence of such high-energy particles is a considerable challenge for our contemporary understanding. At γ-ray energies the bremsstrahlung continuum from electrons is dominant below 1 MeV and again significant in the 10–50 MeV range. When ions over a few hundred MeV/nuc are produced, their interactions with the ambient medium produce pions whose decay products lead to a broad-band continuum at photon energies above 10 MeV (with a broad peak around 70 MeV from neutral pion decay photons; e.g. [58]). Also produced are neutrons which, if energetic enough, may escape from the Sun and be directly detected (e.g. [7]). Typically this radiation is observed after an initial period when a steeper photon spectrum indicates the presence of primary accelerated electrons to tens of MeV (e.g. [57]). All observations of pion decay photons have come so far from very large flares. It is unclear if this is because only large flares accelerate ions to GeV energies, or because of instrumental sensitivity limitations. Sensitivity is clearly not the only reason: the quantitative analysis of a few events exhibiting significant pion production generally led to the conclusion that the ion energy distribution does not have a simple power-law form from the γ-ray line emitting energy domain (1–10 MeV) to the pion producing energy domain above 300 MeV, but may involve breaks and cutoffs (e.g. [1, 9, 25, 26, 57]).

A different, and hitherto unexploited, tool to probe relativistic electrons and positrons in flares is their gyrosynchrotron emission at far infrared wavelengths (THz frequencies). The emission may be generated by the most energetic electrons (tens to hundreds of MeV) produced in solar flares, or by relativistic positrons resulting from nuclear reactions of high-energy protons and γ-particles (>300 MeV/nuc). The sub-mm spectrum from solar flares (frequencies above 100 GHz) was, until recently, expected to be the continually decreasing extension of the gyrosynchrotron spectrum from mildly relativistic electrons observed for many years at cm-mm wavelengths. However, new observations brought a major surprise: in the largest flares the spectrum starts to increase with decreasing wavelength (see e.g. [24]). Interestingly, these events are also found to be associated with significant pion-decay radiation [54]. The origin of this new component is hotly debated. One possibility is that this emission is produced by synchrotron emission from pion-decay positrons [36, 50, 53]. This interpretation is supported by the unique observation combining spatial information of the emission at 210 GHz with emission from energetic ions in the γ-ray line domain. Figure 3 shows two time intervals during the 28 October 2003 flare. The top panel shows the period during which strong pion production is seen. Impulsive emission at 210 GHz (red cross, top panel) shows a strong correlation with the site of interacting ions (pink contours) in the South ribbon of the flare. The lower panel shows the decay phase of the flare during which the 210 GHz emission changes both shape and location, appearing to arise from an extended source between the flare

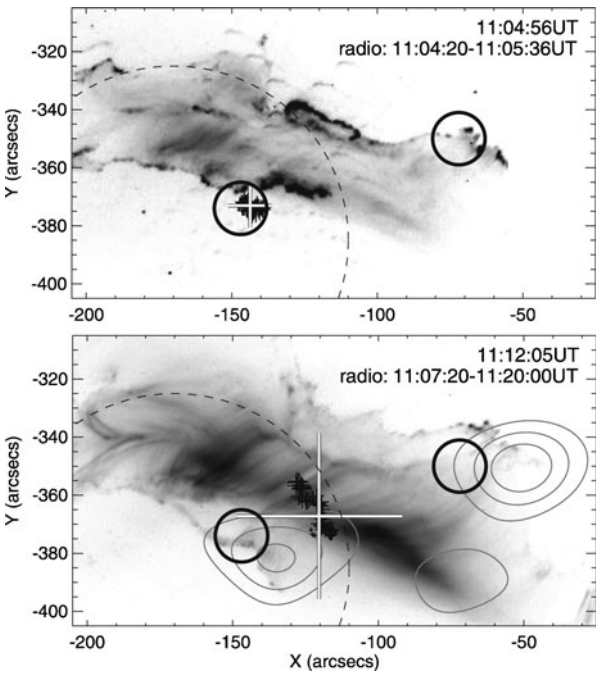

Fig. 3 Superposed images of TRACE (UV; *grey-scale*), RHESSI (*blue* 250–450 keV, *pink* 2.223 MeV) contours from [21] and KOSMA (210 GHz, *red crosses*) during a large solar flare (adapted from [54])

ribbons. The blue contours show two HXR footpoints at this time and a fainter possible coronal source. However, while the close correlation in time and space of the impulsive sub-mm emission and the strong production of neutral pions suggests synchrotron emission from charged pion-decay positrons, the sub-mm flux predicted from the number of positrons derived from charged pion decay seems inadequate to account for observed fluxes. The alternative interpretation (e.g., [50, 54]) that the sub-mm emission is gyrosynchrotron emission from non-thermal electrons would then suggest that electrons in different energy ranges are accelerated in different regions. These, as well as the other interpretations have a number of weaknesses [12], and observations into the THz range are required to provide additional constraints.

Why SPARK? SPARK will explore the gamma-ray spectrum up to the highest energies ever observed by solar-dedicated instruments (∼150 MeV), will have simultaneous context observations of the plasma-magnetic field structures that host the regions of acceleration and emission, and make entirely novel observations in the far infra-red range. SPARK will thus provide an unprecedentedly complete set of observational constraints on the high-energy end of solar particle acceleration. SPARK will provide vital new constraints on γ-ray line spectra (including line shapes and fluences), and for the first time provide access to diagnostics of ions in the 0.1–1 MeV range. The expected improvements in imaging in both the HXR and GRL domain will allow us to address the important question of the location of electron and ion interaction regions. Combined with chromospheric vector magnetography SPARK will possess unique tools to help us relate the electron and ion precipitation sites to the overlying coronal magnetic structure in which the particles are accelerated.

2.3 Non-solar science

Besides particle acceleration at the Sun, SPARK will be able to address energetic photon emissions from terrestrial and astrophysical sources, and thereby enable novel interdisciplinary approaches to the understanding of radiation mechanisms and particle acceleration in different environments. Although the γ-ray instruments on the Compton Gamma Ray Observatory (CGRO) and Fermi spacecraft have greater sensitivity to higher energy γ-rays than SPARK, these are not solar dedicated missions and thus are unable to provide systematic studies over as wide a range of events of different size as SPARK can.

Terrestrial Gamma-ray Flashes (TGFs) are sub-millisecond bursts of gamma-rays up to tens of MeV associated with lightning, discovered by the BATSE instrument on CGRO [11]. There is a consensus on the fundamental emission mechanism of TGFs—bremsstrahlung from relativistic electrons accelerated in DC fields by sub-Dreicer acceleration with avalanche multiplication. But the cause-and-effect relation of TGFs with lightning, the meteorological context, and other important aspects of the physics are still largely unknown and a field of very active study. TGFs generally saturate

orbiting detectors [13], yet still deliver only tens to hundreds of counts because of their brief duration. SPARK's γ-ray instrument will combine extremely large area, high energy range, and extremely high throughput due to the fast LaBr3 scintillators which means that, if properly triggered, it would record by far the best TGF spectra ever seen. This would allow thorough modeling of the spectra of individual events instead of just ensemble averages (e.g., [10]). We would then, for the first time, be able to calculate the range of production altitudes, intrinsic luminosities, and beaming characteristics of TGFs.

γ-ray bursts (GRBs) are the most energetic explosions in the universe, but the γ-ray emission mechanism remains controversial. The prompt emission and subsequent afterglow are believed to be generated by synchrotron radiation in the relativistic jet, which should generate high polarization [60]. The unshielded nature of SPARK's γ-ray detectors offers opportunities to detect polarization signatures of γ-ray bursts (GRBs), and, with appropriate off-axis calibration provision, high quality measurements of the X-ray and γ-ray spectra of the bursts. This can be used to probe the GRB jet structure and the γ-ray emission mechanisms.

The greatly increased sensitivity of SPARK's SXR imager relative to previous SXR instruments, combined with the high sensitivity of its HXR imagers, and better constrained coronal magnetic field modelling, also offer the possibility of tighter constraints on the presence of an X-ray axion signature. Current theories relating to the search for dark matter include the possibility that axions may have a significant role, but robust detections of these particles have yet to be made. Axions are believed to be produced in the solar core and escape almost freely with a small probability of converting into X-ray photons as a result of interactions with the magnetic field [49]. The strength of the coupling constant between axions and the magnetic field is unknown, and attempts to detect an X-ray signal associated with axion conversion in the range 1–15 keV are challenging due to the large background [5, 14].

3 Observable parameters and general measurement strategy

In order to constrain the particle acceleration mechanisms at work in the solar atmosphere it is necessary to make direct measurements of the physical conditions present in (a) the energy release and acceleration sites, and (b) the environment in which the accelerated particles propagate and deposit their energy. SPARK will achieve this through the combination of imaging and spectroscopy in wavelengths that sample the vast range of energies over which particle acceleration signatures are observed, combining high spectral, spatial and temporal resolution.

SPARK will measure the chromospheric and photospheric magnetic field vector at 0.28 and 0.56 arcsec angular resolution respectively and, through high cadence imaging of the photosphere, provide details of the energetic particle precipitation process. The vector field measurements will provide vital information on the evolution of the magnetic field through the atmosphere

and its role in the initiation of the energy release and subsequent evolution. The combined vector field measurements will enable coronal magnetic field extrapolations to be better constrained, critical for the identification of structures such as coronal nulls and quasi-separatrix layers that are central to the particle acceleration process. High resolution imaging in the photosphere (WL), chromosphere (UV and HXR) and corona (SXR) will supply important information on energy partition, and the spatial scales on which the accelerated particles deposit their energy.

The properties of the accelerated particle spectra will be probed through the combination of high resolution HXR and γ-ray spectra and observations in two bands in the FIR. Through the combination of magnetography with imaging in the SXR, HXR, γ-ray and FIR range SPARK will be able to separate transport effects from changes in the acceleration process, providing an unprecedented opportunity to observe and constrain the particle acceleration processes operating in the solar atmosphere. Spatially resolved HXR and γ-ray observations are required to determine the location, spectrum, directivity and temporal evolution of the accelerated ions and electrons. On the Sun there are good reasons to believe that the acceleration region lies in the tenuous corona, while the strongest signatures of the accelerated particles are observed in the lower and denser chromosphere. Current indirect HXR imaging instruments have limited dynamic range that makes it impossible for them to simultaneously image X-rays produced by electrons in or close to the acceleration site at the same time as in the sites where the particles precipitate, and thus to deconvolve the properties of the acceleration mechanism from transport effects. An improvement in sensitivity and dynamic range of order 50–100 is required in order to make this possible. This improvement can be achieved through the use of direct HXR imaging techniques employing grazing incidence optics. Simultaneous observations of coronal and chromospheric HXR emission will, for the first time, allow us to deconvolve the effects of propagation and changes in acceleration, thus allowing us to determine the characteristics of the acceleration process. In addition, measurements of HXR polarization will provide critical data on the anisotropy of the electron distribution that carries so far unexploited information on the properties of the acceleration mechanism.

While the temporal variation of ion and electron acceleration signatures are often closely coupled on the Sun, the large difference in the charge to mass ratio of the two species makes it likely that different processes are responsible for their acceleration. The observed spatial offset of HXR and γ-ray sources observed by RHESSI [20] also suggests this may be the case. High sensitivity and high spectral resolution observations of γ-ray lines (e.g. neutron capture, nuclear de-excitation and positron-annihilation) can provide information on the spectrum, directivity and composition of accelerated ions, as well as on the properties of the interaction region. SPARK will provide such measurements. γ-ray imaging observations from RHESSI have provided important and tantalizing clues to the differences between the precipitation sites of the accelerated ions and electrons in a small number of events that could be studied, but only

time integrated images in the 2.23 MeV line have been obtained. The increased sensitivity of SPARK's γ-ray imaging spectrometer will provide a step change in our ability to image γ-rays, allowing us to produce a time series of images during X and high M-class flare events. This will provide vital clues to the relationship between ion and electron acceleration mechanisms, and strong constraints for current models. Solar flares have never been imaged before in the FIR range. SPARK will make these ground-breaking observations by imaging the solar disk on two detectors in two spectral bands, after spectral selection and splitting.

The observable parameters necessary for SPARK to achieve its science goals must include:

*Simultaneous high temporal (*10*s of seconds) and spatial (sub-arcsecond) resolution measurements of the vector magnetic field in the chromosphere and photosphere* These measurements are required to determine the magnetic environment where particles are accelerated via modelling of the coronal field. Chromospheric magnetic field measurements are an essential new achievement, which is required for more realistic coronal magnetic field extrapolations, because the chromosphere cannot be considered as a force-free boundary. This is an overarching contribution to all science questions addressed by SPARK.

High spectral and temporal resolution photon spectra in the energy range 4 *keV*–150 *MeV* These measurements are the key to establishing energy spectra of accelerated electrons and protons, extending to beyond 100 MeV in order to identify spectral signatures of relativistic protons and to low energies where the non-thermal electron spectra join the thermal background.

Simultaneous images in the range 1 *keV*–30 *MeV capable of viewing faint and bright X-ray and* γ*-ray sources within the same field of view* These observations provide source localisations for both electrons and ions, and contain at low energies the likely transition between non-thermal and thermal electron populations, as a crucial ingredient to investigating the role of non-thermal particles in the energetics of the solar atmosphere. The imaging of nuclear line emissions, together with the extended spectroscopy addressed in the previous item, ensure the substantial improvement of the radiative diagnostics of protons intended to be achieved with SPARK.

*The brightness distribution of the Sun in two far IR wavelength ranges (*25–45 *and* 80–130 μm*)* This is a first in solar flare observations, intended to open the FIR spectrum as a novel diagnostic of the electrons, and possibly positrons, of the highest energies produced in solar flares. Furthermore, thermal bremsstrahlung in this range is an alternative tool to probe energy transport during flares, because it ties the response of the chromosphere to energy deposition coming from the corona.

Measurements of the X-ray polarization in the energy range 5–200 *keV and* γ*-ray imaging polarimetry between* 300–1000 *keV* This long-neglected diagnostic will provide a unique perspective on the angular distribution of high-energy accelerated electrons.

High spatial and temporal resolution images of the photosphere in the 300–530 *nm range* These will reveal the transfer of energy and momentum to the lowest layers that can be reached by a flare. In the context of the other observation this diagnostic will provide constraints on the extension and location of the energy release sites, and will show how flare-accelerated particles relate to the still poorly understood white-light signatures of flares and to the dynamical photospheric phenomena revealed by sunquakes.

The SPARK payload is designed to provide synchronized observations that address very specific science questions and we envisage that the instruments will observe the same targets the majority of the time. However, two of the instruments (HXR focusing imager and vector magnetograph) have a FOV smaller than the Full Sun and thus will require target selection. Targets will be selected on the basis of synoptic data recorded both by SPARK itself as well from other space missions and ground-based observations.

SPARK will focus keenly on large particle acceleration events, and we envisage two classes of science operational mode: "vigil" and "event". Because of the rapidly developing nature of SPARK's targets for observing particle acceleration, the science planning will make use of Near Real Time (NRT) data from the mission, as well as from other observational sources. Observations should be able to be initiated in real-time, as well as through an uploaded schedule. On-board automation will be employed, in that a signal from the science payload will be used to trigger the transition from vigil mode (VMO) to event mode (EMO) observing. Additionally, data selection will be used to constrain telemetry such that the most desired data are given highest priority.

4 Overview of proposed payload elements

The SPARK instrument suite is comprised of five instruments: DESIR (Detection of Solar Eruptive Infrared Radiation); ChroME (Chromospheric Magnetism Explorer); DuPLEX (Dual Passband Low Energy X-ray Imager); Super-FOXSI (Super Focusing X-ray Solar Imager) and LISSAN (Large Imaging Spectrometer for Solar Accelerated Nuclei). The instruments will provide unprecedented coverage of the EM spectrum, from the FIR (105 μm) to high-energy γ-rays (150 MeV), which will enable new methods for exploring the origins of particle acceleration processes in the solar atmosphere and other astrophysical environments. SPARK will provide simultaneous high temporal and spatial resolution measurements of the photospheric and chromospheric magnetic field through the use of the combined action of Hanle and Zeeman effects; spectroscopic imaging over the range 4 keV–30 MeV; high spatial and temporal resolution imaging of the full Sun in the range 1–3.5 keV; the

brightness distribution of the solar atmosphere in two FIR wavelength bands (25–45 and 80–130 μm), high resolution spectroscopy in the range (150 keV–150 MeV) and measurements of the x-ray polarization in the range 5–200 keV. All the payload instruments are based on significant previous design heritage, and thus represent low risk. However, their combined return will produce a step change in our understanding of the fundamental physics involved in particle acceleration in a range of environments. In the following subsections we describe each of the proposed instruments in turn, and in Table 1 we summarize their performance and resources.

4.1 DESIR (Detection of eruptive solar infrared radiation)

DESIR is a two-bandwidth radiometer which provides full-disk observations of the Sun in the far infrared domain. The instrument images the solar disk on two detectors in the spectral bands 25–45 μm and 80–130 μm, after spectral selection and splitting. DESIR is an un-cooled instrument using thermal detectors (micro-bolometer matrices). The design is one that was developed at LESIA/Observatoire de Paris in the framework of the SMESE micro-satellite project. SMESE was declared ready for a phase B study by CNES, but not continued for programmatic and financial reasons.

Sunlight enters the instrument through a thermal filter [ThF] that rejects most of the visible and near infrared part of the flux (26 W for a pupil of 150mm in diameter). A primary mirror (off-axis parabola) [PrM] collects the flux and makes a first image. This image can be intercepted by a shutter [Sh] that can close the instrument cavity in order to perform internal calibration. A secondary mirror [SdM] (also an off-axis parabola) collimates the beam in order that a dichroic filter [DicF] separated the two bands. Each channel comprises a band pass filter [35BPF] [105BPF] and a mirror (off-axis parabola) [35FM] [105FM] that focuses the images on detectors [35Det] [105Det]. The electronics drive both detectors and convert the video signal to digital format, ready to be sent or recorded. The images are analyzed in real time in the processor and stored in case of flare occurrence. A schematic of the conceptual design is show in Fig. 4.

The science objective is to detect minimum flare fluxes of 10^{-18} Wm^{-2} Hz^{-1} (10^4 SFU). Taking into account the instrument performances and noise sources, the signal-to-noise ratio is 80 for the 35 μm channel and 2.5 for the 105 μm channel. Flare detection can be performed on-board by the 35 μm channel, or through the use of a flare flag, and a sophisticated ground data-handling system will permit detection at 105 μm to be achieved. The pointing accuracy requirement is 0.1 deg, with a stability of 2.4 arcsec/ 0.1 s. The regular data rate (corresponding to watching mode) is: 0.024 Mbits/s. The peak data rate (corresponding to the DESIR internal mass memory dump) is: 3.4 Mbits/s. The maximum data telemetry volume is: 5 Gb/day.

DESIR can operate in several different modes, including: non-operating; stand-by; calibration; operating; observation:watching mode; low data acquisition rate—to detect the occurrence of a flare, or flare mode - if a flare has been

Table 1 Payload resource and performance summary

Instrument	DESIR	ChroME	Super-FOXSI	LISSAN	DuPLEX
Energy/	25–45 μm	279.6 ± 1.5 nm	4–60 keV	5–200 keV	1–3.5 keV
λ range	80–130 μm	525.2 ± 1.5 nm		0.15–150 MeV	2.5–3.5 keV
Spatial	50″ @ 35 μm	0.3″ @280 nm	8″	1″ FHWM	2.5″
resolution		0.56″ @520 nm		8″ FWHM	
FOV	50′	307 × 307″	12′	Full sun	Full sun
Spectral	Broadband	50 mÅ @ 280 nm	1 keV @ 4 keV	1 keV @ 6 keV	Broadband
resolution		95 mÅ @ 520 nm	1.5 keV @ 60 keV	15 keV @ 150 keV	
				1.5% FHWM	
				@ 6.1 MeV	
Exp. time	0.1 s	0.5 s	Photon counting	Photon counting	1 s
Data rate	Peak: 3.4	0.7	2	0.8	Peak: 27.5
Mbits/s	Low: 0.012			0.2–7 GB/day	Low: 2.75
Detector	ULIS UL 02051	APS/CCD	400 μm	La Br3 (γ)	APS/CCD
	160 × 120 pix	2k × 2k (Mg)	pixelated CdTe	CdTe (HX)	4 k × 4 k
	35 μm pitch	1k × 1k (Fe)			
Eff. focal	0.27 @ 35 μm	1.375 @ 280 nm	10–15	N/A	2.7
length (m)	0.15 @ 105 μm	0.74 @ 520 nm			
Dimensions	32 × 33.8 × 51	150 × 45 × 50	30 × 20 × 200	10 × 10 × 350 (HX)	45 × 45 × 300
cm^3			30 × 20 × 1500	75 × 75 × 350 (γ)	
Mass (kg)	19.7	52	220	405	66
Power (W)	38.9	55	72	Peak: 163	48
				Average: 81	
Absolute	0.1 deg	35″	1′	5′	1′
pointing					
Pointing	2.4″/0.1 s	10″/30 s	Internal	Internal	2.0″/0.1 s
stability					

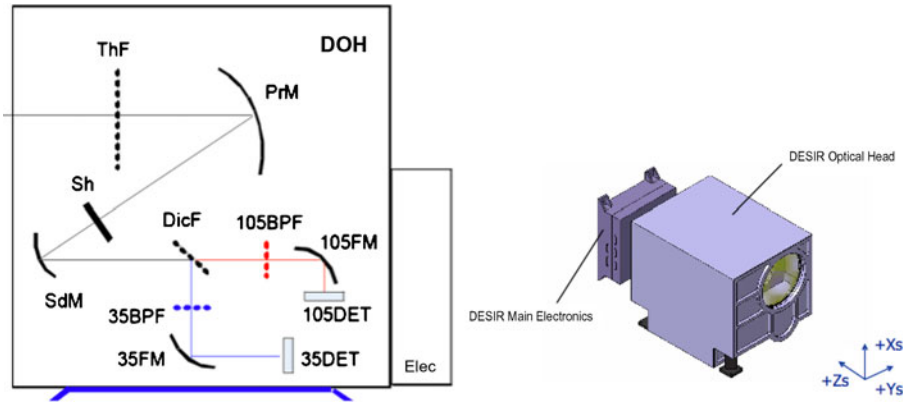

Fig. 4 *Left* Conceptual design of the DESIR Optical Head (DOH). Sunlight enters from the left through the thermal filter [ThF]. *Right* DESIR mechanical layout

detected in watching mode, images are stored in the DESIR internal mass memory at high cadence. The shutter can be closed to calibrate the thermal background.

4.2 ChroME (Chromospheric Magnetism Explorer)

ChroME is designed to simultaneously measure the chromospheric and the photospheric magnetic field vector. The filtergraph type instrument allows the polarization state of the light to be quantified down to a level of 10^{-4} of the continuum intensity in the chromospheric Mg II k 279.6 nm line and a photospheric line in the visible, the baseline choice being the Fe I 525 nm line. The polarization signal is created by the Zeeman effect, atomic level polarization, scattering polarization and is modified by the Hanle effect. The theoretical modeling of these effects allows the retrieval of vector magnetic field maps in the chromosphere and the photosphere simultaneously.

A schematic of the ChroME concept is shown in Fig. 5. ChroME consists of a 250 mm aperture Gregorian telescope with a heat rejection system at the prime focus. An active secondary mirror (M2) is used for correlation tracking and re-focusing. Instrumental polarization is minimized by placing the polarimetry unit before any inclined optical surface. The filtergraph comprises a double Fabry-Perot interferometer that provides constant spectral resolution over the whole field of view. A dichroic beam splitter then distributes light to each channel. The final spectral selection is performed by pre-filters. The use of the etalons allows simultaneous observations to be made in the chromospheric and the photospheric channel through adjustment of the free spectral range (FSR).

ChroME is capable of achieving a spatial resolution of 0.28″, spectral resolution of 50 mÅ and a signal-to-noise ratio (SNR) of 300 per 0.15″ pixel in the chromospheric channel. The nominal cadence is 30 s for 15 wavelength

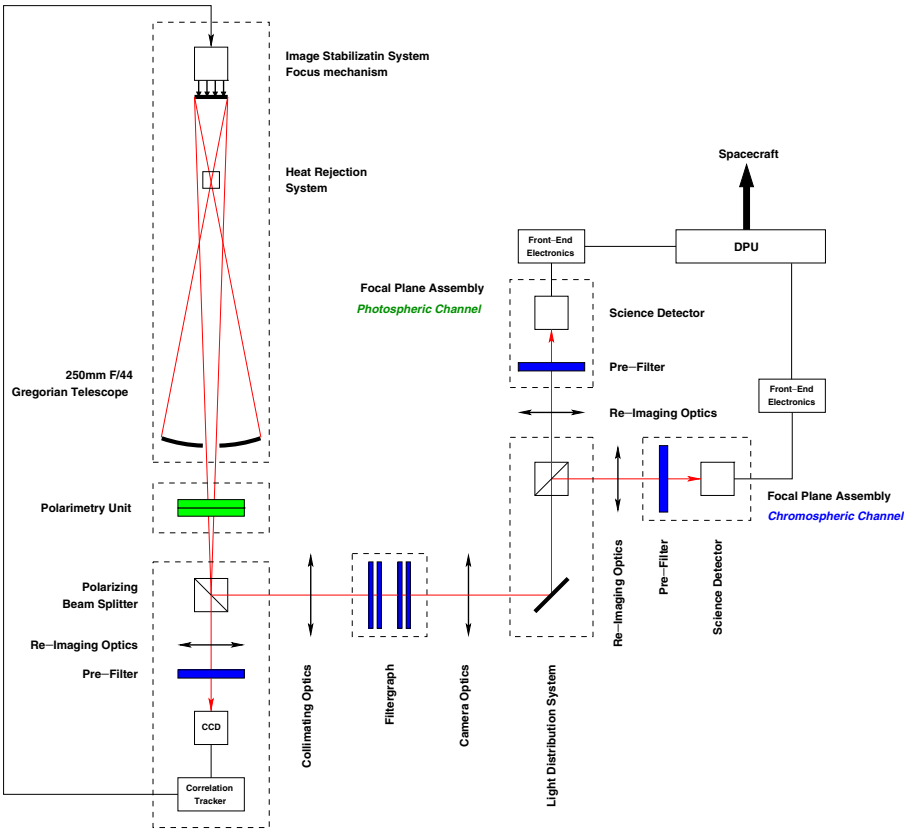

Fig. 5 Schematic representation of ChroME

positions, and the field of view is approximately 300 × 300 arcsec. The SNR can be significantly enhanced by longer exposure times, and on-board or post-facto spatial binning, allowing for a SNR of better than 2000. Reducing the number of wavelength samples, or on-board spatial pixel binning can be used to obtaining higher time cadence. The photospheric channel is envisaged to operate approximately in the 300 to 530 nm range, with the Fe I 525 nm line the most likley choice. A spatial resolution of 0.56″ in this channel. This line provides reliable photospheric vector magnetograms (e.g. [51]) as well as imaging of white light flares. Calculations of the photon budget based on measurements of the solar irradiance [6], theoretical calculations of the Zeeman signal of the Mg II k line (Pietarila 2010, private communication) and the scattering polarization signal modified by the Hanle effect [55] indicate a polarimetric sensitivity of 3.2×10^{-3} for the Stokes parameters in active regions.

The data rate for simultaneous measurement of the chromospheric and photospheric vector field in 30 s would be 15 MB/s. On-board data selection

and compression can reduce this to 700 kbit/s. The polarimetric calibration will be performed prior to launch and the in-flight calibration will require dark images, flat-fields and a measurement of the straylight. The polarimetric calibration can be maintained through comparison with ground-based observations.

ChroME is also part of the payload of the Solar Magnetism Explorer (SolmeX, see [43]). However, to provide a complete description of the SPARK payload we include a similar description here.

4.3 Super-FOXSI (Super Focusing Optics X-ray Solar Imager)

Super-FOXSI uses grazing incidence focusing optics to image directly in HXR over the energy range 4–60 keV with a spectral resolution of 1 keV and a spatial resolution of ∼8 arcsec. Current HXR imaging measurements are obtained through non-focusing rotation modulation collimator (RMC) imaging techniques [19], such as those used on RHESSI [35]. However, these, and other types of non-focusing imaging methods, have three main limitations that can be overcome by the use of focusing optics: effective area; large non-solar background, and limited dynamic range. The dynamic range for RMC imaging is limited by emission from the entire field of view. For focusing optics, the dynamic range (and resolution) is set by the shape of the point spread function (PSF), thus the sharper the PSF, the better the dynamic range. Current HXR focusing optics already provide a dynamic range >50 (indirect imaging methods such as RHESSI <30), which with appropriate calibration procedures can be increased to >100 for events with good statistics. For well-separated sources, this range can be extended to >1000.

The current version of FOXSI [31] is comprised of 7 telescope modules, each with 7 nested shells and a 2 m focal length. Seven 128 × 128 double-sided silicon strip detector cover each of the 7 detector planes. The strip size is 75 μm. Combined with a 2-m focal length, the effective pixel size is 7 arcsec. The energy resolution of FOXSI is ∼0.6 keV with a low energy threshold of ∼5 keV. FOXSI has a field of view of approximately 640 × 640 arcsec (HPW) that covers slightly less than a quarter of the solar disk. The current typical angular resolution (FWHM) achievable for modules containing multiple nested shells is 8 arcsec.

Super-FOXSI will be an updated instrument that uses similar modules to FOXSI. The effective area will be increased by a longer focal length, by filling the modules with the largest possible number of shells (which almost doubles the effective area at 10keV and adds response to higher energies), by using multilayer coatings and by increasing the diameter of the instrument. A total effective area of 400 cm^2 at 40 keV (as shown in Fig. 6) is achievable for an instrument mass of 200 kg. Figure 7 shows the instrument concept. For the proposed second flight of FOXSI, the Si strip detectors will be replaced with 60 μm CdTe strip detectors. CdTe detectors have already been investigated by ISAS for the HXI system on Astro-H and tests of 400 μm pitch CdTe detectors have resulted in an energy resolution of 1.5 keV at 60 keV, an angular

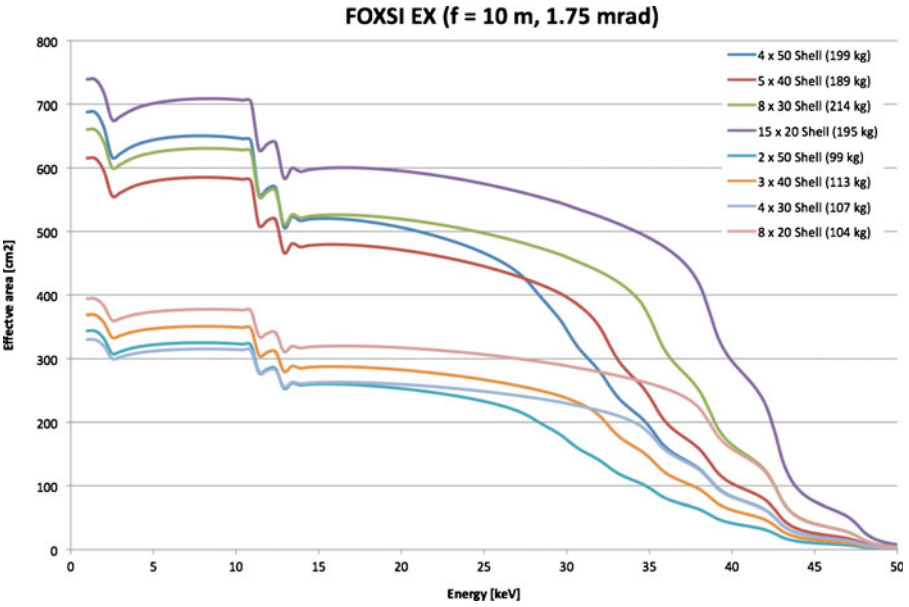

Fig. 6 FOXSI effective area as a function of energy. The FOXSI optics assembly is modular, providing many design options. The figure shows different module configurations optimized for energies up to 40 keV. A 10 m focal length is used, no multilayers are considered

resolution <10 arcsec and a low-energy cut-off of 2 keV. The 60 μm pitch detector that will fly on the updated FOXSI payload has been fabricated and its spectral resolution is currently being evaluated. Hence, small pitch CdTe strip detectors will be available on the timescale of SPARK. A long focal length of the order of 10–15 m is highly preferable in order to improve the high energy response of the telescope. Expandable booms of such length are used for the NuSTAR mission (NASA SMEX) that will be launched in 2012.

Indirect imaging techniques in this energy range have an effective area that is proportional to detector area, and thus high sensitivity requires large detectors that are difficult to shield against non-solar background. CdTe

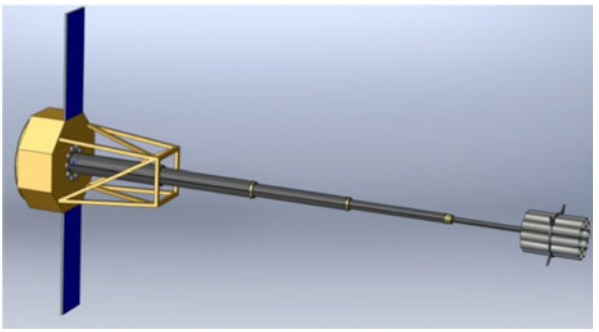

Fig. 7 Super-FOXSI strawman instrument concept with expandable boom (STEREO heritage) and 7 telescope modules

detectors now provide high QE in the HXR range with pixel sizes $\leq$500 μm, corresponding to approximately 10 arcseconds on the Sun for a 10 m focal length (e.g. NuSTAR). Development for pixel sizes of 250 μm is underway. Currently existing Si or CdTe strip detectors provide spatial information (pixel size) down to 1 arcsec. In comparison to RHESSI, the area sensitive to the non-solar background is 10^{-6} smaller, which when combined with active shielding would produce a negligible non-solar background. Together with the larger effective area, Super-FOXSI will be about 50–100 times more sensitive at 40 keV than RHESSI (0.08 ph cm^{-2} s^{-1} keV^{-1}) enabling coronal HXR sources, microflares and electrons escaping from the acceleration region to be imaged. The angular resolution (FWHM) of such a telescope system would be ∼8 arcsec, the same resolution as most of the published RHESSI images, and improvements in technology are likely to lead to improvements on a ten-year timescale. In addition, Super-FOXSI images will not be subject to reconstruction noise or imaging artefacts.

The pointing stability of Super-FOXSI is not critical as long as absolute changes in pointing are known. Hence, the pointing can change in time, but it must be measured by an aspect system for correction during data analysis. Such a system is in use on the NASA RHESSI and NuSTAR missions. Super-FOXSI will operate primarily in a synoptic mode once pointed at a suitable target. During large flares, attenuators will move in front of the detectors to reduce the count rate at lower energies. Similar attenuators are used for the RHESSI mission, and also for STIX onboard Solar Orbiter.

4.4 LISSAN (Large Imaging Spectrometer for Solar Accelerated Nuclei)

LISSAN combines two sensors in order to provide indirect imaging and spectroscopic information in the HXR and γ-ray regimes. The γ-ray sensor performs γ-ray spectroscopy (150 keV to ∼150 MeV) with high-resolution scintillators (LaBr3). Imaging over this range is produced by placing pairs of grids above the detectors that produce Moire patterns on the detector surfaces; these patterns can be resolved by coarsely segmenting the detectors. This is an indirect (Fourier) imaging technique closely related to that used on the Yohkoh HXT imager and planned for the STIX instrument for Solar Orbiter. For LISSAN, in order to modulate photons across the entire energy range of interest, the grids are made from tungsten slats 3 cm deep. LISSAN's HXR sensor uses the same imaging technique in a much smaller package with cadmium zinc telluride (CZT) detectors and lightweight grids. The HXR sensor, with energy range ∼5 keV to 200 keV, bridges the energy gap between LISSAN and FOXSI (60–150 keV), a particularly important range for understanding the nonthermal component in large flares, which often feature a downward break in this band that is not yet understood. Compared to the gamma-ray sensor, the lower energy range allows for much finer grids, and the LISSAN HXR sensor will be able to image down to 1″ FWHM, producing the sharpest solar images ever produced in the non-thermal high-energy band for

comparison with optical and (E)UV data. The HXR sensor is closely based on the STIX design for Solar Orbiter.

In its baseline configuration (see Fig. 8), LISSAN's γ-ray sensor will consist of 20 detector modules, 16 of which sit below grid pairs. The other four double the sensitivity for spectroscopy, since they do not have the ~75% attenuation associated with the grids in the other 16 modules; thus imaging and spectroscopic sensitivity needs are efficiently balanced. Each module is made up of sixteen "fingers" of scintillator, 2.5 × 2.5 cm in cross-section and 10 cm deep. In one direction, this segmentation allows the Moire pattern to be resolved. Segmentation in the other direction improves polarization sensitivity, since polarization is measured by counting coincidences (Compton scatters) between detector segments, and also improves light collection and therefore spectral resolution in each detector, since a phototube or Si avalanche photodiode at the back end can very effectively collect all the scintillation light from each "finger". This guarantees the energy resolution (better than 1.5% FWHM at 6.1 MeV) needed to measure the Doppler profiles of the C and O lines at 4.4 and 6.1 MeV. LISSAN can also function as an imaging polarimeter from 300 to 1000 keV. Scaling from RHESSI's polarization analyses by taking the relative energy ranges, detector areas and geometry into consideration (but neglecting systematic errors in a non-rotating instrument), LISSAN should

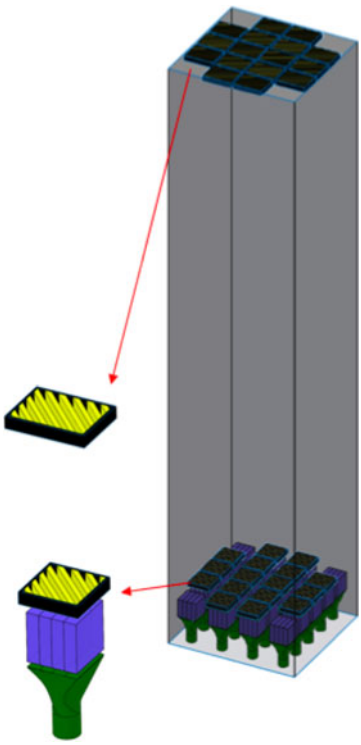

Fig. 8 Schematic of a LISSAN γ-ray sensor

have a polarization sensitivity about 4 times better than RHESSI for a given event. Boggs et al. [4] found that the 3-sigma polarization sensitivity of RHESSI for the X4.8 flare of July 23, 2002, was 27%, measuring 21% ± 9% for that event.

With this instrumental configuration we expect to be able to image ion interaction sites in the 2.2 MeV line from neutron capture down to flares of GOES class approximately M3 (ion content can be calculated down to flares another order of magnitude fainter). For X-class flares, LISSAN will produce up to a few dozen frames, showing the evolution of ion interaction sites with time during the flare. The C and O nuclear lines, whose Doppler profiles indicate the angular distribution and He/H ratio in accelerated ions at the interaction site, will have sufficient statistics for meaningful analysis of flares of magnitude M5 and higher. The finest grids in the gamma-ray sensor will allow imaging down to 8″ FWHM, a resolution more than adequate for separating foot-point pairs and able to resolve foot-point sizes in some cases. LISSAN will achieve 40× the sensitivity achievable currently with RHESSI (5 counts/cm^2) and 1.5% dE/E at 6.1 MeV (compared to <10 keV for RHESSI) and a range of 100 keV −150 MeV (compared to 17 MeV for RHESSI) and 40× what RHESSI achieves (50 counts/cm^2) in the 2.2 MeV neutron capture line.

The dimensions of the γ-ray sensor are 75 × 75 cm square by 3.5 meters in length (3.0 m grid separation). The HXR sensor will have the same length but a much smaller cross-section. Electronics and high-voltage supply boxes are expected to total no more than 1/3 of a cubic meter in total, and possibly much less, depending on the degree of miniaturization achieved for the electronics of the γ-ray sensor. There will be 320 1″ photomultiplier tubes (PMTs) and analog electronics chains for the gamma-ray sensor (as part of the instrument definition phase we will conduct a trade study on the question of replacing the conventional PMTs with silicon avalanche photodiodes). Peak power for the system is 163 W, including margin. Outside of flares, the current draw of the high-voltage side, the analog electronics, and the ADC will be much lower at 81 W with margin. The entire HXR sensor requires a total power of less than 3 W, since it uses low-power solid-state detectors and ASIC electronics.

Data volume and telemetry requirements are highly compressible. A RHESSI-like data mode, in which each photon count in each segment is separately recorded as a 4-byte data record, is optimum scientifically but would produce approximately 20 GB of data for the largest (X10+) flares. If all data were taken down in this mode the rate would be roughly 7GB/day. It would be desirable to retain accumulated spectra on a cadence of about 10 minutes for gain and background calculations, for a continuous data volume of 200 MB/day. With a full-Sun field of view, LISSAN's pointing and alignment requirements are low. For aspect for both its sensors, LISSAN uses a high-cadence, sub-arcsecond, grid-embedded aspect system similar to RHESSI and so does not rely on spacecraft pitch/yaw aspect. Spacecraft roll aspect (to ∼1′) is used after the fact, however, to assist in establishing the azimuthal position of the flare on the Sun. Pointing accuracy of 5′ is sufficient to enable all LISSAN science. The most sensitive alignment parameter for this imaging technique

is the relative twist of the front and rear grids. This requirement will be less severe than that which was successfully achieved for RHESSI's grids.

4.5 DuPLEX (Dual Passband Low Energy X-ray telescope)

DuPLEX makes use of two sets of nested grazing-incidence mirrors to focus soft X-rays onto two detector arrays: one in the range 1–3.5 keV; the other in the range 2.5–3.5 keV. Selecting shallower grazing incidence angles in the higher-energy channel allows some tuning of the telescope effective area to peak at higher energies. Filters between the focal plane and detectors are then used to further control the band-pass of each energy channel, allowing selection of the energy ranges above. The mirrors are coated, which increases throughput substantially. However, above 3.5 keV this falls off in absolute terms and hence in order to maintain high signal-to-noise at high cadence, the high energy cut-off is restricted to 3.5 keV. The Images are formed on two spatially offset detector arrays at the focal plane of each telescope half to allow simultaneous imaging of plasma as it thermalizes during a particle acceleration event, and the overlapping energy ranges provide the possibility for the use of ratios to identify the plasma at the higher end of the energy range.

DuPLEX builds on the experience of Hinode's X-Ray Telescope (XRT), which operates in the 6–200 Å range with two filter wheel mechanisms. To remove the need for filter-switching mechanisms so that both energy channels can be captured simultaneously, we have opted for a dual-hyperboloid design: two sets of mirrors, each forming a semi-circular segment in cross-section, will focus X-rays of different energy ranges onto neighbouring focal planes at the rear of the instrument. Offsetting the axes of symmetry of the low- and high-energy half-shells allows us the separation of the optic axes so that each channel can be imaged on a separate detector. In addition, using three shells in each mirror assembly more than compensates losses in effective area by using only semi-circular cross sections.

The function of DuPLEX is to image the thermal emission of very hot ($T > 10^6$ K) plasma. By providing high-dynamic range images in the SXR range, it will bridge the gap between the smaller-FOV instruments (ChroME and Super-FOXSI) and the lower resolution, but also full-Sun LISSAN and DESIR. DuPLEX will provide crucial information on the plane-of-sky magnetic topology in the hot corona, allowing us to better constrain the relationship between non-thermal and thermal emission from the area around the reconnection site. The structure of DuPLEX is a carbon fibre reinforced polymer (CFRP) cylinder of length 3000 mm, diameter 450 mm, with CFRP baffle between the two telescope segments. At the front of the telescope, arc-shaped, aluminium/polyimide filters render the telsecope solar-blind, i.e., sensitive only to incoming X-rays. Incident X-rays enter the telescope through these filters. Two sets of adjacent hyperboloid shells are housed at the front of the telescope to bring X-rays to a focus at the rear of the instrument, 2700 mm from the front of the primary mirror assembly. Large FOV systems in the X-ray range have been studied more carefully in recent years, thanks to a

desire for exploitation in extra-solar astronomy and the advances of ray-tracing and computation methods for optical calculations. The problem of optimising resolution is well known in this domain. DuPLEX's design can achieve a best on-axis resolution of 2.5–3.0″, with a FOV-averaged resolution of 5″ within 15′ of the axis. In this way, we are able to image the soft X-ray thermal emission of post-reconnection plasma across most of the solar disc, while also retaining some thermal information about sources far from SPARK's principle target. The usefulness of this mode in locating flares for triggering is also open to exploitation. Beyond the mirror assemblies, a band-pass filter in each telescope half constrains the instrumental response. DuPLEX uses a beryllium filter of thickness 30 μm in the high-energy channel, and an aluminium mesh filter of thickness 160 nm in the lower energy channel. The detector arrays are located at the rear of the instrument and consist of two silicon CCD arrays arranged side-by-side at the focal planes of the X-ray telescope. Due to the variation in spatial resolution across the 70′ field of view, the detector array will be actuated in the direction parallel to the telescope axis, to allow for correction to the focus. Such a mechanism has already been used successfully in Hinode/XRT. The plate scale of the telescope is tuned such that pixels subtend 1″ on the sky, permitting oversampling of the image. A shutter mechanism in front of each detector will be responsible for controlling the exposure time of each detector array, since different exposure times may be required in each channel. The instrument concept is shown in Fig. 9.

Hinode/XRT uses uncoated, polished Zerodur mirrors to achieve its focusing of incident X-rays. Throughput estimates are based on this design, in the knowledge that mirrors coated with gold or iridium would provide higher reflectivity by a factor 10 at 2 keV, and a factor 500 at 3 keV. Such higher throughputs allow a more detailed study of higher-temperature plasma, and imply a substantial dynamic range, arguing for 14- or 16-bit readout. The effective area is 50 cm^2 at 2.6 keV and >2.0 cm^2 in the range 1.7–2.3 keV.

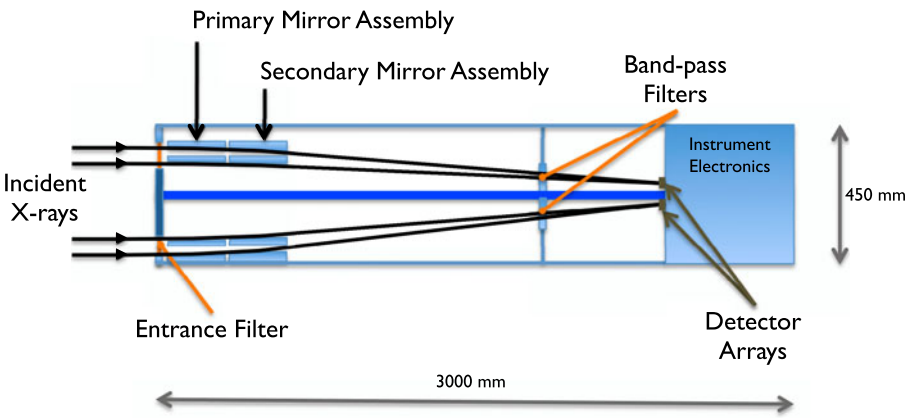

Fig. 9 Plan view of DuPLEX showing envelope and optical system

In order to remove the need for an independent pointing mechanism DuPLEX uses a large (2.2 solar diameter) FOV, centred on the spacecraft pointing. The large FOV of the DuPLEX design contains some margin to allow for misalignment in flight through integration limitations and structural creep. Nonetheless, its large FOV means that pointing accuracy is of low concern. Pointing stability is somewhat more constrictive, but provided that the telescope is stable to 2.0″ in 0.1 s (typical minimum exposure time), this criterion will be satisfied. The data rate for DuPLEX is 2.8–28 Mbps. In order to monitor the short timescales over which particle acceleration evolves, DuPLEX will take images at a 1-second cadence during the flare impulsive phase, streaming these images to a running buffer in on-board storage. However, to keep mean telemetry at a more reasonable level, images can be telemetered to the ground with a 10-second cadence, achieved by on-board summing.

5 Spacecraft concept

Since the payload consists of a number of direct imaging instruments, the spacecraft needs to be three-axis stabilised to allow imaging measurements to be made with minimum spatial blurring. The combination of individual instrument stability requirements means that SPARK needs a stability of 2″ over 0.1 seconds. The accuracy of pointing must be better than 30″ so as to allow ChroME and Super-FOXSI to point their relatively small fields-of-view at the correct target. Knowledge of the pointing must be good to within a few arcseconds, a figure driven by the resolution of DuPLEX. The spacecraft absolute pointing requirement is 60 arcseconds. This can be achieved through the combination of momentum wheels and magnetic torquers for attitude control, and four thrusters for orbit control. The attitude sensors should include a fine Sun sensor and a star tracker in order to determine spacecraft pointing relative to the Sun. An inertial reference unit comprised of four gyros is required to determine changes of attitude with time.

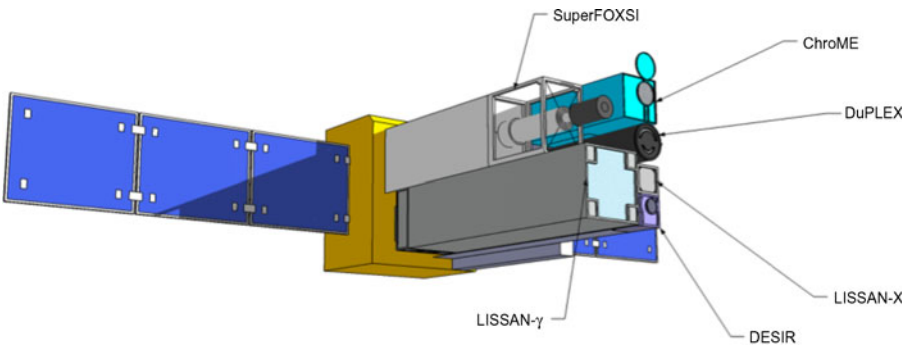

Fig. 10 Schematic of the SPARK spacecraft showing the accommodation of the instruments and the solar panels

The primary design drivers for the spacecraft are the accommodation of the expandable boom required for Super-FOXSI and the large mass of LISSAN. Figure 10 shows a schematic of our spacecraft concept. The spaceraft dimensions are 1.9 m by 4.6 m by 1.6 m, which fits comfortably within the Soyuz fairing. Super-FOXSI's boom is stowed at launch, measuring no more than 2 m by 1 m. The boom will be deployed in orbit and a single use mechanism employed to align the optics. Subsequent deflections in the mast will be monitored by a laser metrology system such as that planned for NuSTAR [17].

5.1 On-board data handling and telemetry requirements

The average data rate for SPARK is around 2 Mbits/s, but there will be substantial variation depending on the observation mode. For example, LISSAN may produce 20 GB data for a large flare, while DESIR's watching mode produces only 0.024 Mbits/s. Flare detection is performed on-board for DESIR and we envisage the use of a flare trigger in DuPLEX in order to implement data selection techniques for it and the other instruments. Given the variation in data rates for different instruments and different modes of observation, SPARK should have the capability to store on-board data obtained prior to and during a large X-class flare. This requires on-board mass memory of approximately 40 GB. Additionally, data selection will be used to constrain telemetry such that the most desired data are given highest priority.

SPARK communications will use a steerable X-band antenna to provide a downlink from the spacecraft for science data download to Earth, and an S-band up and downlink at for commanding and housekeeping. For redundancy we also include 2 S-band omni-directional antennas. An X-band transmitter at 8.4 GHz can support the required 2 Mbit/s data rate.

6 Summary and conclusions

Energetic particles are not a by-product, but a critical component of the universe. They are key to understanding energy conversion and energy transport in explosive situations in astrophysical plasmas, as well as in more gradual and long-lived processes in structures that exhibit e.g. strong gradients and turbulence. Building on several decades of space-borne observations we propose SPARK—a high-energy solar physics mission, which will allow us to deepen our understanding of energetic particle signatures over an enhanced range of energies in the solar atmosphere, from the very low limits in microflares and non-flaring activity to relativistic energies. A crucial test for candidate acceleration processes is the ability to account for signatures over a wide range of spatial, temporal and energy scales. In order to achieve these goals, SPARK will combine high resolution (spatial, spectral and temporal) imaging and spectroscopy in wavelengths that sample the vast range of energies over which particle acceleration signatures are observed, adding context observations of the magnetic field and plasma structures. SPARK will enhance our

understanding of how such processes operate in environments outside of the solar atmosphere, both through direct observation (e.g. TGFs and GRBs) and the indirect application of constraints provided by observations of the solar atmosphere.

References

1. Alexander, D., Dunphy, P.P., MacKinnon, A.L.: High-energy gamma-ray emission from solar flares: constraining the accelerated proton spectrum. Sol. Phys. **151**, 147–167 (1994). doi:10.1007/BF00654088
2. Bamert, K., Kallenbach, R., Ness, N.F., Smith, C.W., Terasawa, T., Hilchenbach, M., Wimmer-Schweingruber, R.F., Klecker, B.: Hydromagnetic wave excitation upstream of an interplanetary traveling shock. ApJ **601**, L99–L102 (2004). doi:10.1086/381962
3. Bentley, R.D., Klein, K.-L., van Driel-Gesztelyi, L., Démoulin, P., Trottet, G., Tassetto, P., Marty, G.: Magnetic activity associated with radio noise storms. Sol. Phys. **193**, 227–245 (2000)
4. Boggs, S.E., Coburn, W., Kalemci, E.: Gamma-Ray polarimetry of two X-class solar flares. ApJ **638**, 1129–1139 (2006). doi:10.1086/498930
5. Carlson, E.D., Li-Sheng, T.: Pseudoscalar conversion and X-rays from the sun. Phys. Lett. B **365**, 193–201 (1996). doi:10.1016/0370-2693(95)01250-8
6. Cebula, R.P., Thuillier, G.O., Vanhoosier, M.E., Hilsenrath, E., Herse, M., Brueckner, G.E., Simon, P.C.: Observations of the solar irradiance in the 200–350 NM interval during the ATLAS-1 mission: a comparison among three sets of measurements-SSBUV, SOLSPEC and SUSIM. GRL **23**, 2289–2292 (1996)
7. Chupp, E.L., Ryan, J.M.: High energy neutron and pion-decay gamma-ray emissions from solar flares. Res. A&A, **9**, 11–40 (2009). doi:10.1088/1674-4527/9/1/003
8. Chupp, E.L., Forrest, D.J., Ryan, J.M., Cherry, M.L., Reppin, C., Kanbach, G., Rieger, E., Pinkau, K., Share, G.H., Kinzer, R.L.: Observation of the 2.223 MeV gamma-ray line on the SMM satellite - the event of 1980 June 7. ApJ **244**, L171–L174 (1981). doi:10.1086/183505
9. Dunphy, P.P., Chupp, E.L., Bertsch, D.L., Schneid, E.J., Gottesman, S.R., Kanbach, G.: Gamma-Rays and neutrons as a probe of flare proton spectra: the solar flare of 11 June 1991. Sol. Phys. **187**, 45–57 (1999).
10. Dwyer, J.R., Smith, D.M.: A comparison between Monte Carlo simulations of runaway breakdown and terrestrial gamma-ray flash observations. GRL **322**, L22804 (2005). doi:10.1029/2005GL023848
11. Fishman, G.J., Bhat, P.N., Mallozzi, R., Horack, J.M., Koshut, T., Kouveliotou, C., Pendleton, G.N., Meegan, C.A., Wilson, R.B., Paciesas, W.S., Goodman, S.J., Christian, H.J.: Discovery of intense gamma-ray flashes of atmospheric origin. Science **264**, 1313–1316 (1994). doi:10.1126/science.264.5163.1313
12. Fleishman, G.D., Kontar, E.P.: Sub-Thz radiation mechanisms in solar flares. ApJ **709**, L127–L132 (2010). doi:10.1088/2041-8205/709/2/L127
13. Grefenstette, B.W., Smith, D.M., Hazelton, B.J., Lopez, L.I.: First RHESSI terrestrial gamma ray flash catalog. J. Geophys. Res. **114**(A13), A02314 (2009). doi:10.1029/2008JA013721
14. Hannah, I.G., Hurford, G.J., Hudson, H.S., Lin, R.P., van Bibber, K.: First limits on the 3-200 keV X-ray spectrum of the quiet sun using RHESSI. ApJ. **659**, L77–L80 (2007). doi:10.1086/516750
15. Hannah, I.G., Krucker, S., Hudson, H.S., Christe, S., Lin, R.P.: An intriguing solar microflare observed with RHESSI, Hinode, and TRACE. A&A **481**, L45–L48 (2008). doi:10.1051/0004-6361:20079019
16. Hannah, I.G., Hudson, H.S., Hurford, G.J., Lin, R.P.: Constraining the hard X-ray properties of the quiet sun with new RHESSI observations. ApJ **724**, 487–492 (2010). doi:10.1088/0004-637X/724/1/487
17. Harrison, F., et al.: SPIE **7732**, 77320S (2010)

18. Holman, G.D., Sui, L., Schwartz, R.A., Emslie, A.G.: Electron bremsstrahlung hard X-ray spectra, electron distributions, and energetics in the 2002 July 23 solar flare. ApJ **595**, L97–L101 (2003). doi:10.1086/378488
19. Hurford, G.J., Schmahl, E.J., Schwartz, R.A., Conway, A.J., Aschwanden, M.J., Csillaghy, A., Dennis, B.R., Johns-Krull, C., Krucker, S., Lin, R.P., McTiernan, J., Metcalf, T.R., Sato, J., Smith, D.M.: The RHESSI imaging concept. Solar Phys. **210**, 61–68 (2002). doi:10.1023/A:1022436213688
20. Hurford, G.J., Schwartz, R.A., Krucker, S., Lin, R.P., Smith, D.M., Vilmer, N.: First gamma-ray images of a solar flare. ApJ **595**, L77–L80 (2003). doi:10.1086/378179
21. Hurford, G.J., Krucker, S., Lin, R.P., Schwartz, R.A., Share, G.H., Smith, D.M.: Gamma-ray imaging of the 2003 October/November solar flares. ApJ **644**, L93–L96 (2006). doi:10.1086/505329
22. Kai, K., Melrose, D.B., Suzuki, S.: Storms. In: McLean, D.J., Labrum, N.R. (eds.) Solar radiophysics: studies of emission from the Sun at metre wavelengths, pp. 415–441. Cambridge Univ. Press (1985)
23. Kašparová, J., Kontar, E.P., Brown, J.C.: Hard X-ray spectra and positions of solar flares observed by RHESSI: photospheric albedo, directivity and electron spectra. A&A **466**, 705–712 (2007). doi:10.1051/0004-6361:20066689
24. Kaufmann, P., Raulin, J.-P., de Castro, C.G.G., Levato, H., Gary, D.E., Costa, J.E.R., Marun, A., Pereyra, P., Silva, A.V.R., Correia, E.: A new solar burst spectral component emitting only in the terahertz range. ApJ **603**, L121–L124 (2004). doi:10.1086/383186
25. Kocharov, L.G., Lee, J.W., Zirin, H., Kovaltsov, G.A., Usoskin, I.G., Pyle, K.R., Shea, M.A., Smart, D.F.: Neutron and electromagnetic emissions during the 1990 May 24 solar flare. Sol. Phys. **155**, 149–170 (1994). doi:10.1007/BF00670736
26. Kocharov, L., Debrunner, H., Kovaltsov, G., Lockwood, J., McConnell, M., Nieminen, P., Rank, G., Ryan, J., Schoenfelder, V.: Deduced spectrum of interacting protons accelerated after the impulsive phase of the 15 June 1991 solar flare. A&A **340**, 257–264 (1998).
27. Kontar, E.P., Brown, J.C.: Solar flare hard X-ray spectra possibly inconsistent with the collisional thick target model. ASR **38**, 945–950 (2006). doi:10.1016/j.asr.2005.09.029
28. Kontar, E.P., MacKinnon, A.L., Schwartz, R.A., Brown, J.C.: Compton backscattered and primary X-rays from solar flares: angle dependent green's function correction for photospheric albedo. A&A **446**, 1157–1163 (2006). doi:10.1051/0004-6361:20053672
29. Kontar, E., Brown, J.C., Emslie, A.G., et al.: Deducing electron properties from hard X-ray observations. Space Sci. Rev. (2011)
30. Krucker, S., Benz, A.O., Bastian, T.S., Acton, L.W.: X-Ray network flares of the quiet sun. ApJ **488**, 499 (1997). doi:10.1086/304686
31. Krucker, S., Christe, S., Glesener, L., McBride, S., Turin, P., Glaser, D., Saint-Hilaire, P., Delory, G., Lin, R.P., Gubarev, M., Ramsey, B., Terada, Y., Ishikawa, S.-N., Kokubun, M., Saito, S., Takahashi, T., Watanabe, S., Nakazawa, K., Tajima, H., Masuda, S., Minoshima, T., Shomojo, M.: The focusing optics X-ray solar imager (FOXSI). SPIE **7437**, 4 (2009). doi:10.1117/12.827950
32. Kundu, M.R., White, S.M., Gopalswamy, N., Lim, J.: Millimeter, microwave, hard X-ray, and soft X-ray observations of energetic electron populations in solar flares. ApJS **90**, 599–610 (1994). doi:10.1086/191881
33. Leach, J., Petrosian, V.: The impulsive phase of solar flares. II - characteristics of the hard X-rays. ApJ **269**, 715–727 (1983). doi:10.1086/161081
34. Lin, R.P., Schwartz, R.A., Kane, S.R., Pelling, R.M., Hurley, K.C.: Solar hard X-ray microflares. ApJ **283**, 421–425 (1984). doi:10.1086/162321
35. Lin, R.P., Dennis, B.R., Hurford, G.J., Smith, D.M., Zehnder, A., Harvey, P.R., Curtis, D.W., Pankow, D., Turin, P., Bester, M., Csillaghy, A., Lewis, M., Madden, N., van Beek, H.F., Appleby, M., Raudorf, T., McTiernan, J., Ramaty, R., Schmahl, E., Schwartz, R., Krucker, S., Abiad, R., Quinn, T., Berg, P., Hashii, M., Sterling, R., Jackson, R., Pratt, R., Campbell, R.D., Malone, D., Landis, D., Barrington-Leigh, C.P., Slassi-Sennou, S., Cork, C., Clark, D., Amato, D., Orwig, L., Boyle, R., Banks, I.S., Shirey, K., Tolbert, A.K., Zarro, D., Snow, F., Thomsen, K., Henneck, R., McHedlishvili, A., Ming, P., Fivian, M., Jordan, J., Wanner, R., Crubb, J., Preble, J., Matranga, M., Benz, A., Hudson, H., Canfield, R.C., Holman, G.D., Crannell, C., Kosugi, T., Emslie, A.G., Vilmer, N., Brown, J.C., Johns-Krull, C., Aschwanden, M., Metcalf,

T., Conway, A.: The reuven ramaty high-energy solar spectroscopic imager (RHESSI). Solar Phys. **210**, 3–32 (2002). doi:10.1023/A:1022428818870
36. Lingenfelter, R.E., Ramaty, R.: On the origin of solar flare microwave radio bursts. Plan. Spa. Sci. **15**, 1303 (1967). doi:10.1016/0032-0633(67)90184-5
37. Liu, C., Wang, H.: Reconnection electric field and hardness of X-Ray emission of solar flares. ApJ **696**, L27–L31 (2009). doi:10.1088/0004-637X/696/1/L27
38. Liu, C., Lee, J., Jing, J., Gary, D.E., Wang, H.: The spatial distribution of the hard X-Ray spectral index and the local magnetic reconnection rate. ApJ **672**, L69–L72 (2008). doi:10.1086/525849
39. Mackinnon, A.L.: Coulomb collisional precipitation of fast electrons in solar flares. A&A **194**, 279–287 (1988)
40. Masuda, S., Kosugi, T., Hudson, H.S.: A hard X-ray two-Ribbon flare observed with Yohkoh/HXT. Sol. Phys. **204**, 55–67 (2001). doi:10.1023/A:1014230629731
41. McTiernan, J.M.: RHESSI/GOES observations of the nonflaring sun from 2002 to 2006. ApJ **697**, 94–99 (2009). doi:10.1088/0004-637X/697/1/94
42. Murphy, R.J., Share, G.H., Grove, J.E., Johnson, W.N., Kinzer, R.L., Kurfess, J.D., Strickman, M.S., Jung, G.V.: Accelerated particle composition and energetics and ambient abundances from gamma-ray spectroscopy of the 1991 June 4 solar flare. ApJ **490**, 883 (1997). doi:10.1086/304902
43. Peter, H., Abbo, L., Andretta, V., Auchere, F., Bemporad, A., Berrilli, F., Bommier, V., Braukhane, A., Casini, R., Curdt, W., Davila, J., Dittus, H., Fineschi, S., Fludra, A., Gandorfer, A., Griffin, D., Inhester, B., Lagg, A., Landi Degl'Innocenti, E., Maiwald, V., Manso Sainz, R., Martinez Pillet, V., Matthews, S., Moses, D., Parenti, S., Pietarila, A., Quantius, D., Raouafi, N., Raymond, J., Rochus, P., Romberg, O., Schlotterer, M., Schuehle, U., Solanki, S., Spadaro, D., Teriaca, L., Tomczyk, S., Trujillo Bueno, J., Vial, J.: Solar magnetism eXplorer (SolmeX). ArXiv e-prints. 2011arXiv1108.5304P (2011)
44. Peterson, L., Winckler, J.R.: Short γ-ray burst from a solar flare. Phys. Rev. Lett **1**, 205–206 (1958). doi:10.1103/PhysRevLett.1.205
45. Ramaty, R., Mandzhavidze, N., Kozlovsky, B., Murphy, R.J.: Solar atmopheric abundances and energy content in flare accelerated ions from gamma-ray spectroscopy. ApJ **455**, L193 (1995). doi:10.1086/309841
46. Ramaty, R., Mandzhavidze, N.: Gamma-rays from solar flares. In: Martens, P.C.H., Tsuruta, S., Weber, M.A. (eds.) Highly Energetic Physical Processes and Mechanisms for Emission from Astrophysical Plasmas. IAU Symposium, vol. 195, pp. 123 (2000)
47. Raulin, J.P., Klein, K.-L.: Acceleration of electrons outside flares: evidence for coronal evolution and height-extended energy release during noise storms. A&A **281**, 536 (1994)
48. Share, G.H. Murphy, R.J.: Gamma radiation from flare-accelerated particles impacting the sun. Washington DC American Geophysical Union Geophysical Monograph Series **165**, 177 (2006)
49. Sikivie, P.: Experimental tests of the 'invisible' axion. Phys. Rev. Lett. **51**, 1415–1417 (1983). doi:10.1103/PhysRevLett.51.1415
50. Silva, A.V.R., Share, G.H., Murphy, R.J., Costa, J.E.R., de Castro, C.G.G., Raulin, J.-P., Kaufmann, P.: Evidence that synchrotron emission from nonthermal electrons produces the increasing submillimeter spectral component in solar flares. Sol. Phys. **245**, 311–326 (2007). doi:10.1007/s11207-007-9044-0
51. Solanki, S.K., Barthol, P., Danilovic, S., Feller, A., Gandorfer, A., Hirzberger, J., Riethmüller, T.L., Schüssler, M., Bonet, J.A., Martínez Pillet, V., del Toro Iniesta, J.C., Domingo, V., Palacios, J., Knölker, M., Bello González, N., Berkefeld, T., Franz, M., Schmidt, W., Title, A.M.: SUNRISE: Instrument, mission, data, and first results. ApJ **723**, L127–L133 (2010). doi:10.1088/2041-8205/723/2/L127
52. Trottet, G., Vilmer, N., Barat, C., Benz, A., Magun, A., Kuznetsov, A., Sunyaev, R., Terekhov, O.: A multiwavelength analysis of an electron-dominated gamma-ray event associated with a disk solar flare. A&A **334**, 1099–1111 (1998)
53. Trottet, G.: In: Fang, C., Schmieder, B., Ding, M.D. (eds.) Third French? Chinese meeting on solar physics, 82. Nanjing Univ. Press (2006)
54. Trottet, G., Krucker, S., Lüthi, T., Magun, A.: Radio submillimeter and γ-ray observations of the 2003 october 28 solar flare. ApJ **678**, 509–514 (2008). doi:10.1086/528787

55. Trujillo-Bueno, J.: Spectropolarimetric investigations of the magnetization of the quiet-sun chromosphere. MmSAI **81**, 681 (2010)
56. Vilmer, N., Trottet, G., Barat, C., Schwartz, R.A., Enome, S., Kuznetsov, A., Sunyaev, R., Terekhov, O.: Hard X-ray and gamma-ray observations of an electron dominated event associated with an occulted solar flare. A&A **342**, 575–582 (1999)
57. Vilmer, N., MacKinnon, A.L., Trottet, G., Barat, C.: High energy particles accelerated during the large solar flare of 1990 May 24: X/γ-ray observations. A&A **412**, 865–874 (2003). doi:10.1051/0004-6361:20031488
58. Vilmer, N., MacKinnon, A.L., Hurford, G.J.: Properties of energetic ions in the solar atmosphere from γ-ray and neutron observations. Space Sci. Rev. (2011). doi:10.1007/s11214-010-9728-x
59. Vink, J.: Multiwavelength signatures of cosmic ray acceleration by young supernova remnants. In: Aharonian, F.A., Hofmann, W., Rieger, F. (eds.) American Institute of Physics Conference Series, vol. 1085, pp. 169–180. (2008)
60. Yonetoku, D., Murukami, T., Gunji, S., et al.: arXiv:1010.5305 (2010)
61. Zharkova, V.V., Kuznetsov, A.A., Siversky, T.V.: Diagnostics of energetic electrons with anisotropic distributions in solar flares. I. Hard X-rays bremsstrahlung emission. A&A **512**, A8 (2010). doi:10.1051/0004-6361/200811486